Lawrence Berkeley National Laboratory
Lawrence Berkeley National Laboratory

Title
VIRTUAL PHOTOPRODUCTION OF HIDDEN AND OPEN CHARM

Permalink
https://escholarship.org/uc/item/5945w35k

Author
Clark, A.R.

Publication Date
1980-11-01

Peer reviewed

MasTeR

VIRTUAL PHOTOPRODUCTION OF HIDDEN AND OPEN CHARM

A.R. Clark, K.J. Johnson, L.T. Kerth, S.C. Loken, T.W. Markiewicz,
P.D. Meyers, W.H. Smith, M. Strovink, and W.A. Wenzel

Physics Department and Lawrence Berkeley Laboratory
University of California, Berkeley, California 94720

R.P. Johnson, C. Moore, M. Mugge, and R.E. Shafer

Fermi National Accelerator Laboratory
Batavia, Illinois 60510

G.D. Gollin[a], F.C. Shoemaker, and P. Surko[b]

Joseph Henry Laboratories, Princeton University
Princeton, New Jersey 08544

presented by M. Strovink

A. Introduction

I shall begin by describing the Berkeley-Fermilab-Princeton multi-muon spectrometer and the techniques used to analyze the data which it has collected. Notwithstanding the title of this talk, the first physics topic in fact will be relevant to weak interactions, the subject of this conference. Drawing from results now being prepared for publication[1], I shall present limits on the cross section with which possible heavy neutral or doubly charged muons are produced via right-handed charged currents. Turning to heavy-quark muoproduction, I shall outline next the relevant phenomenology, emphasizing the prediction of the vector dominance (VMD) and photon-gluon-fusion (γGF) models. The first heavy-quark data to be discussed will be the dimuon-mass spectrum observed in trimuon final states, which provides our published[2] limit on muoproduction of the Υ family. The bulk of the quarkonium results are devoted to $J/\psi(3100)$ muoproduction. After briefly reviewing our original ψ results[3], I will focus on a combined analysis of the polarization and Q^2-dependence of elastically produced ψ's. These data have recently been submitted for publication[4]. The balance of my talk will be devoted to the muoproduction of open charm, observed in events with two muons in the final state. We have published[5] the cross-sections for diffractive charm muoproduction and photoproduction, and also the corresponding charm structure function and its substantial contribution to inclusive scale-noninvariance[6]. The conference organizers have asked that inclusive structure-function results not be emphasized here. Preliminary inclusive data from this experiment were reported at the 1979 Lepton-Photon Symposium[7].

Before proceeding, it is fitting to note that the Berkeley-Fermilab-Princeton experiment is to an unusual extent the product of graduate-student research. The heavy-muon and Υ production limits, ψ results, and open-charm data presented here form part of the Ph.D.

theses, respectively, of Wesley Smith, Thomas Markiewicz, and George Gollin.

## B. Experimental Method

The muon spectrometer achieved the desired integrated luminosity ($\geq 10^6$ nb^{-1}) by using a massive target (~ 5 kg/cm^2). High acceptance over the full target length made necessary a spectrometer magnet integral with the target. Its steel plates functioned also as hadron absorbers for calorimetry and muon identification. Full acceptance was maintained in the forward direction, with no blind "beam hole". Inability to find all the final state muons otherwise would have altered drastically the interpretation of many events. A dipole field configuration, requiring only one pair of coils for the full magnet, was most compatible with high forward acceptance. Proportional and drift chambers were able to withstand the full beam flux at Fermilab (typically 2×10^6 muons per 1-sec spill) without deadening in the beam area.

Construction of the apparatus depicted in Fig. 1 was completed in 1977. It consisted of 18 25-ton modules each containing 5 10-cm thick steel plates, 5 calorimeter scintillators (omitted in modules 16-18), and a pair of proportional (PC) and drift chambers (DC)[8]. Banks of 12 trigger scintillators (S_1-S_{12}) were located in even modules 4-18. The fiducial volume, 1.8×1 m^2 in area, extended 16 m in the beam direction. Within the central 1.4×1 m^2 area of each magnet plate, the 19.7 kgauss field was uniform to 3% and mapped to 0.2%. Located upstream of module 1 were one additional PC and DC, 63 beam scintillators, 8 beam PC's and 94 scintillators sensitive to accidental beam and halo muons.

Beam muons were momentum-analyzed by systems of proportional chambers and scintillator hodoscopes interspersed between magnets producing two separate beam deflections. Pulse heights from calorimeter counters within the spectrometer provided a tentative longitudinal ver-

MULTI-MUON SPECTROMETER

BERKELEY-FERMILAB-PRINCETON
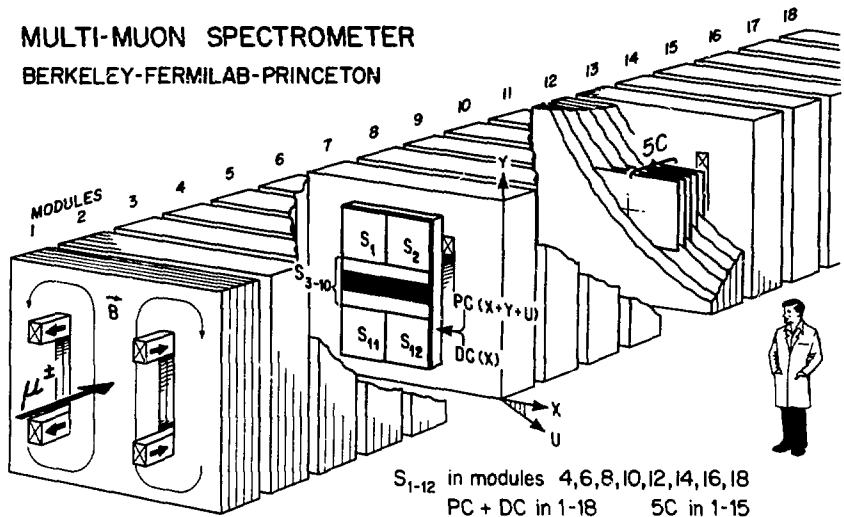
S_{1-12} in modules 4,6,8,10,12,14,16,18
PC + DC in 1-18   5C in 1-15

XBL 795-9605

FIG. 1. Sketch of the multimuon spectrometer. The spectrometer magnet, serving also as a target and hadron absorber, reaches 19.7 kG within a $1.8 \times 1 \times 16$-m^3 fiducial volume. Over the central $1 \times 1 \times 16$ m^3, the magnetic field is uniform to 3% and mapped to 0.2%. Eighteen pairs of proportional (PC) and drift chambers (DC), fully sensitive over 1.8×1 m^2, determine the muon momenta typically to 8%. The PC's register coordinates at 30° (u) and 90° (y) to the bend direction (x) by means of 0.5-cm-wide cathode strips. Banks of trigger scintillators (S_1-S_{12}) occupy eight of the eighteen magnet modules. Interleaved with the 10-cm-thick magnet plates in modules 1-15 are 75 calorimeter scintillators resolving hadron energy E_{had} with rms uncertainty $1.5E_{had}^{\frac{1}{2}}$ GeV. Not shown upstream of module 1 are 1 PC and DC, 63 beam scintillators, 8 beam PC's, and 94 scintillators sensitive to accidental beam and halo muons.

- 3 -

tex position. The beam track then was traced forward to this vertex using the PC and DC hits. Outgoing tracks were recognized initially at their downstream end. Hits were added extending the tracks upstream to the vertex, making adequate allowance for Coulomb scattering and momentum uncertainty. In order not to interfere with rejection of halo tracks or later use of outgoing tracks to pinpoint the vertex, the transverse vertex position was not allowed to influence this upstream projection. At least 4 PC hits in two views and 3 hits in the third view were required for each accepted track. The small electromagnetic showers found along high energy muon tracks in iron, due mainly to direct production of electron pairs, contributed extra hits in the wire chambers which were not completely rejected at this stage. After the full track was identified, it was possible to apply a momentum-fitting algorithm capable of solving for the Coulomb-scattering angle in each magnet module, yielding a rigorous χ^2 for the track. By iteration, this algorithm identified and suppressed the false extra hits.

The beam and secondary tracks next were examined for consistency with a common vertex. The vertex position was moved by iteration in 3 dimensions to minimize the overall χ^2 while including all associated tracks. After the vertex was fixed, the coordinates and momentum of each track were redetermined, subject to the condition that it intersect the vertex point.

For analysis of 3μ final states the events were subjected to a 1-constraint fit demanding equality between the beam energy at the interaction point and the sum of muon and hadron shower energies in the final state. Using error matrices produced by the fits to individual tracks, the constraint perturbed all components of each track momentum. The resulting momentum resolution is 7%-12% (typically 8%) per track. At the ψ mass, the dimuon mass resolution is 9%. The uncertainty in Q^2 typically is 10%, but is bounded below by ~ 0.15 (GeV/c)^2 because of track

- 4 -

angle uncertainty.

The acceptance and resolution of the spectrometer were modeled by a complete Monte Carlo simulation. Coordinates of randomly sampled beam muons were used to represent the beam. Simulated muons underwent single and multiple Coulomb scattering, bremmstrahlung, and other energy-loss straggling in each magnet plate and were bent by the precisely mapped field. Simulated interactions occurred between muons and nucleons in non-degenerate Fermi motion, or coherently between muons and Fe nuclei. At low momentum transfer the effects of nuclear shadowing were taken into account. Coherent and elastic processes were attenuated by the appropriate form factors even for forward scattering (at $|t|_{min}$). Detector resolutions and efficiencies were included throughout. Monte Carlo events were output in the same magnetic tape format as raw data, and were reconstructed, momentum-fit and histogrammed by the same programs.

Data were accumulated during the first half of 1978 using $\sim 4 \times 10^{11}$ (gated) 209 GeV muons, of which approximately 90% were μ^+. Results presented here are based on 75% of this sample, except for the open-charm results, which represent 50% of the data.

C. Limits on Muoproduction of Heavy Neutral or Doubly Charged Muons

Considerable speculation has been devoted to the possible existence of heavy neutral gauge leptons. Variations of the standard $SU(2) \times U(1)$ model[9] have been proposed in which the known lepton doublets are coupled[10] to an M^0 or in which both right- and left-handed doublets exist and include[11] M^0's. Grand unification schemes frequently introduce M^0's, e.g. those[12] which embed $SU(2)_L \times U(1)_R$ in $SU(3)_L \times SU(3)_R$. In addition to the M^0, heavy doubly charged gauge muons (M^{++}) have been proposed in the context of an extended $SU(2) \times U(1)$ theory in doublets with the known singly charged leptons[11].

There exist few experimental limits on the masses of heavy muons.

- 5 -

Studies of π and K decay[13] exclude the M^0 mass from the range $m_\mu < m_{M^0} < m_K$. Ref. 14 sets a 90%-confidence lower limit of 1.8 GeV/c^2 on the mass of the heavy muon M^-. Although there are 90%-confidence lower limits of[15] 2.4 GeV/c^2 and[16] 8.4 GeV/c^2 on the M^+ mass, the strongest experimental constraint on the M^0 mass is the limit[17] $m_{M^0} > 1$ GeV/c^2.

Possible evidence for M^0 production has arisen from three experiments. Two $\mu^- e^+$ events produced by $\nu_\mu N$ interactions below 30 GeV in the SKAT bubble chamber were attributed[18] to the production of an M^0 with $1.4 < m_{M^0} < 2.4$ GeV/c^2. In a cosmic ray experiment[19] deep underground, five events were analyzed as evidence for a heavy lepton with mass 2-4 GeV/c^2. Originally the observation of neutrino-induced trimuon events at Fermilab[20] prompted their interpretation as examples of M^0 production. Further experiments and analyses have failed to develop corroborating evidence for the interpretation of these phenomena as examples of M^0 production.

Using the simplest parton model with single W^+ exchange, invoking the Callan-Gross relation and considering only $\Delta S = \Delta C = 0$ processes and isoscalar tragets,

$$\frac{d^2\sigma(\mu^+(L.H.)N \to \bar{M}^0 X)}{d\nu dy} = (\frac{g_R}{g})^2 \frac{G^2 E m_N F_2(x)}{\pi y}$$

where $\nu = Q^2/s$, (1-y) is the fraction of t'.· laboratory muon energy retained by the $\bar{M}^0$, and g_R/g is the ratio of possible right-handed to left-handed current amplitudes. The differential cross section is independent of $\bar{M}^0$ mass, except for kinematic restriction of the allowed area of the Q^2-ν plane. The differential decay rate for $M \to \mu^+ \mu^- \bar{\nu}_\mu$, where the $\bar{M}^0$ is coupled to the μ^+ by a (V+A) current, is

$$\frac{d^5\sigma(\bar{M}^0 \to \mu^+ \mu^- \bar{\nu}_\mu)}{dx_- dx_\nu d\phi_\nu d\cos\theta_\nu d\phi_-} \propto x_\nu (1-x_\nu)(1-P\cos\theta_\nu).$$

Here $x_-(x_\nu)$ is $2p_{c.m.}/m_{M^0}$ for the $\mu^-(\bar{\nu}_\mu)$, θ_ν and ϕ_ν define the c.m. $\bar{\nu}_\mu$ direction relative to the $\bar{M}^0$ direction, θ_- and ϕ_- define the c.m. μ^-

direction relative to the $\bar{\nu}_\mu$ direction, and P is the $\bar{M}^0$ polarization along its direction of motion. Since the $\bar{M}^0$ carries the left-handed polarization of the incident μ^+, the two muons are emitted preferential- ly forward and together carry an average of 80% of the $\bar{M}^0$ energy in the laboratory.

Monte Carlo events were generated according to the above formulae at lepton masses of 1,2,3, 6,9,12 and 14 GeV/c^2, and were binned[21] in Q^2 and in $p_\perp$, the daughter muon momentum transverse to $\vec{Q}$. Kinematic cuts were chosen individually for each heavy lepton type and mass in order to exclude data while retaining Monte Carlo M events. An empirical contour then was drawn for each Q^2-$p_\perp$ plot in order to contain all the data events on the low $p_\perp$, low Q^2 side. The Monte Carlo event popu- lations on the high $p_\perp$, high Q^2 side of the contours then provide the cross section limits.

Figure 2 displays the mass-dependent limits[1] on $\bar{M}^0$ and M^{++} produc- tion. Also indicated are the expected products of cross section and branching ratio for the production of $\bar{M}^0$'s and M^{++}'s, where the $\mu\mu\nu$ branching ratio is assumed to be 0.1 and 0.2 for $\bar{M}^0$ and M^{++}, respect- ively. To 90% confidence the data exclude the production of an $\bar{M}^0$ and M^{++} coupled with Fermi strength to a right-handed current in the mass range $1<m_M<9$ GeV/c^2. Without a special mechanism to suppress pair pro- duction, doubly-charge leptons in this mass range would have been de- tected at PETRA. No comparable limits on M^0 production are available.

D.   Phenomenology of Heavy-Quark Production by Muons

The theoretical framework for discussion of charm leptoproduction is evolving rapidly. In 1976 Sivers, Townsend and West[22] obtained a lower bound on the total ψN cross-section, requiring measurement of the ratio of cross-sections for forward ψ and total charm photoproduction. This bound depends only on unitarity and OZI[23] rules. Adding tradi- tional vector-meson dominance (VMD) assumptions makes the ratio of
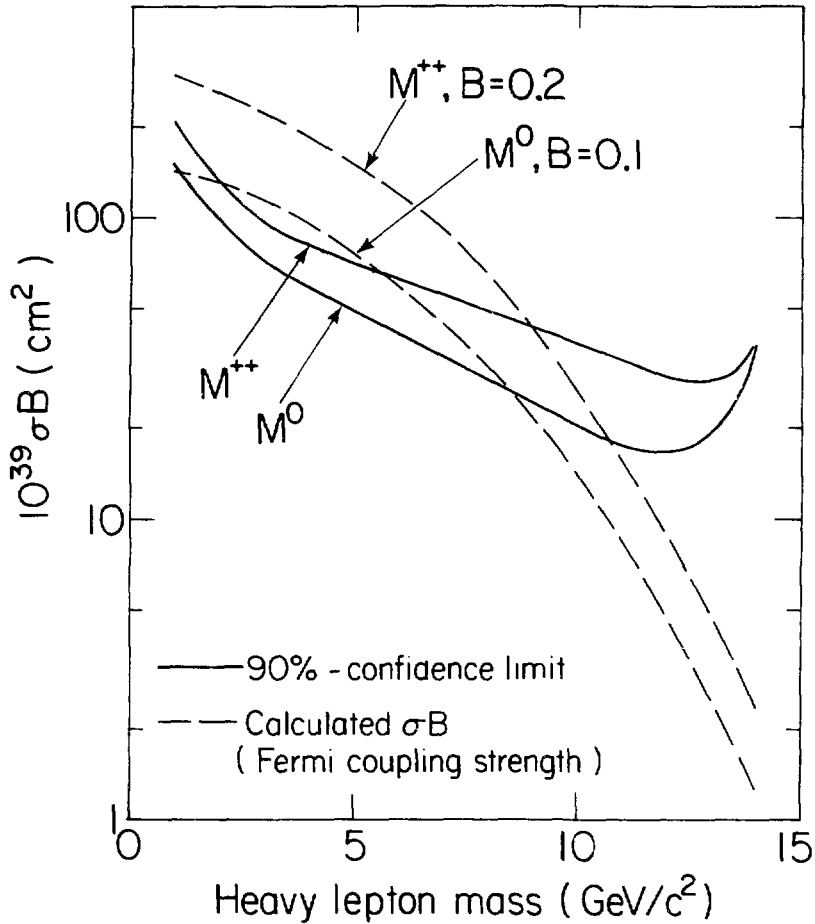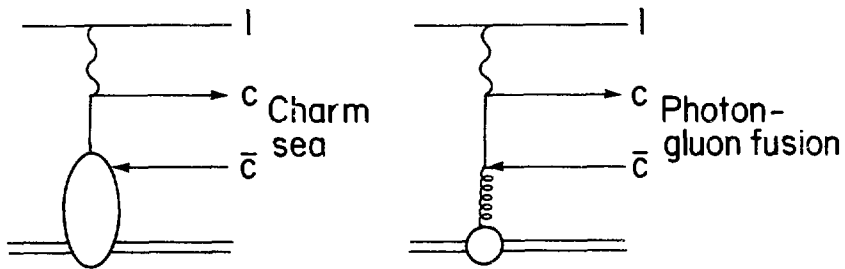
XBL 809-2016

FIG. 2. Experimental upper limits and calculated cross section-branching ratio products σB for heavy-muon (M^0 and M^{++}) production by 209-GeV muons, plotted vs. heavy muon mass. The calculation assumes $B(M \to \mu\mu\nu)=0.1$ (M^0) or 0.2 (M^{++}), and right-handed coupling of μ^+ to $\bar{M}^0$ with Fermi strength. With these assumptions, to 90% confidence the data rule out the existence of M^0 or M^{++} with mass between 1 and 9 GeV/c².

elastic to total ψN cross-sections nearly equal to the ratio of elastic

ψ to total charm photoproduction. This ratio is evaluated in Ref. 22

as $(0.013\pm0.004)/\lambda$, where $\lambda\approx0.7$ is an off-shell correction. VMD con-

nects charm photoproduction to muoproduction via a $(1+Q^2/m_\psi^2)^{-2}$ ψ propa-

gator. The original data[24] on charm muoproduction were analyzed using

a "photon dissociation" model of Bletzacker and Nieh (BN)[25].

    With the advent of quantum chromodynamics, recent activity has

centered on the photon-gluon-fusion (γGF) model[26], to which the right-

hand graph in Fig. 3 refers. This is a Bethe-Heitler diagram for

charmed-quark pair production with the nuclear photon replaced by a

gluon. Not shown are the additional (presumably) soft gluon exchanges

needed to conserve color. Comparison with the graph at left emphasizes

the close connection between photon-gluon-fusion and the charmed sea.

The large mass m_c associated with the internal quark line makes the

gluon-exchange diagram finite and possibly the leading contributor to

the charmed sea. Specific use of that mechanism makes it possible to

allow sensibly for threshold effects due to m_c, and to predict the

experimentally important correlation between the momenta of the two

charmed quarks. In particular, the γGF model unifies the description

of closed and open charm production via the quark pair mass $m_{c\bar{c}}$:

charmonium production is taken to be dual to $c\bar{c}$ production with

$2m_c<m_{c\bar{c}}<2m_D$, while open-charm production has $m_{c\bar{c}}>2m_D$. This makes the

γGF charmonium calculations much more sensitive to m_c than are the open-

charm calculations. Typically, one assumes $m_c=1.5$ GeV/c^2 and

$\alpha_s=1.5/\ln(m_{c\bar{c}}^2/\Lambda^2)$ with $\Lambda=0.5$ GeV/c^2. The distribution in gluon momentum

fraction x is usually taken to be $3(1-x)^5/x$, with the exponent set by

counting-rule arguments[27] and the coefficient by the integral over

Bjorken $x_B=Q^2/2m_p\nu$ of the measured inelastic structure function

$F_2(x_B,Q^2)$. The fraction of charmonia realized as the ψ is perhaps best

regarded as a fit parameter[28] with the value 1/6. With these choices,

C Charm
C̄ sea

C Photon-
C̄ gluon fusion

XBL 809-2015

FIG. 3. Illustration of the similarity between the "parton" picture in which the virtual photon is absorbed by a quark in the charmed sea, and the "photon-gluon-fusion" mechanism for pair production of heavy quarks. The latter process can be viewed as a prescription for generating the charmed sea, which predicts as well the correlation between $c(x)$ and $\bar{c}(x)$.

at 209 GeV the total cross section for (presumably primarily elastic) ψ muoproduction is 0.47 nb, and for open $c\bar{c}$ muoproduction is 5.0 nb. A similar calculation with bottom quarks of mass 4.7 GeV/c^2 and charge 1/3 gives 0.28 pb for T muoproduction at 275 GeV, or 0.13 pb at 209 GeV.

E. Limit on T Muoproduction

Figure 4 displays the spectrum in dimuon mass $M_{\mu^+\mu^-}$ from this experiment[2]. Events below 5 GeV/c^2 in $M_{\mu^+\mu^-}$ were reconstructed and momentum fit as previously described in Ref. 3. Above 5 GeV/c^2, the analysis of all events was checked by a hand reconstruction which was blind to the invariant mass. At all masses the assignment of beam-sign secondary muons either to the scattered muon or to the produced muon pair is the critical decision in the analysis. Incorrect pairing of muons from ψ or muon trident production can cause events which properly belong in the low-mass region to be misinterpreted as having a higher mass. Our muon pairing algorithm was selected primarily to minimize this problem. The scattered muon is chosen to be the one with the smaller value of the square of its scattering angle divided by its scattered energy. The alternative choice for the scattered muon would produce more than a one-order-of-magnitude exaggeration of the high-mass continuum near the T, as shown by the "mispaired" histogram segment in Fig. 4.

Despite the care exercised in muon pairing, Monte Carlo studies show that there remains a significant contribution in the region $4.7 < M_{\mu^+\mu^-} < 8.4$ GeV/c^2 from incorrectly analyzed lower-mass events. Allowance for these effects is most reliably made by use of an empirical fit to the mass continuum. The extrapolated continuum contains 1.8 ± 1.0 background events in the T region $8.4 < M_{\mu^+\mu^-} < 11.1$ GeV/c^2, which in fact includes two observed events. With 90% confidence, there are fewer than 3.8 events above the extrapolated background.

The simulated T mass resolution and detection efficiency are 9%
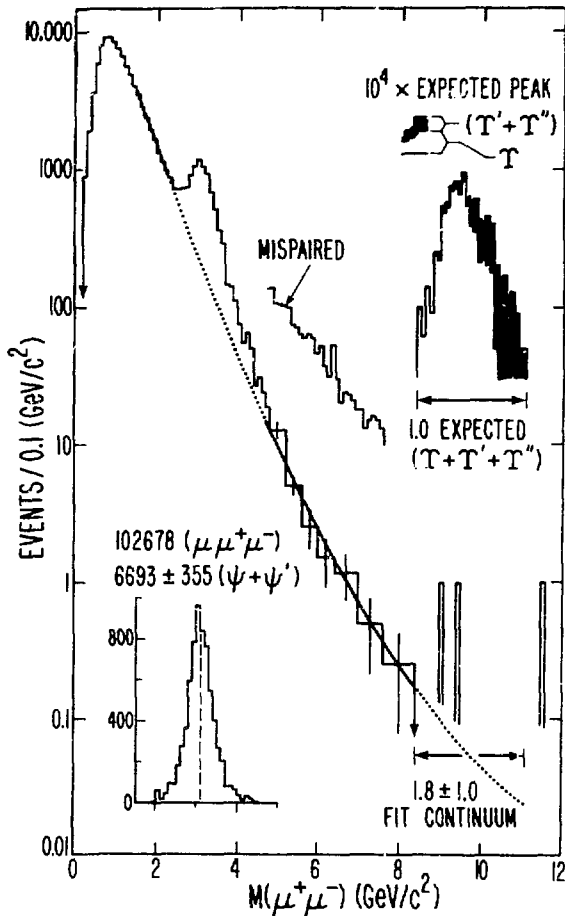
- 11 -

FIG. 4. Spectrum of 102 678 dimuon masses from 75% of the trimuon data. The background is fit by $\exp(a+bM+cM^2)$ in the regions of the solid curve with a χ^2 of 13.7 for 14 degrees of freedom, and is extrapolated along the dotted curve. The "mispaired" histogram segment illustrates the appearance of the mass spectrum if the alternative muon-pairing choice is made. The background-subtracted ψ peak is shown in the lower corner; the expected peak from $10^4\times$ the Monte-Carlo simulated T, T´, and T´´ sample is shown in the upper corner, with the contribution from T´ and T´´ in black. The extrapolated continuum contains 1.8 ± 1.0 background events in the T region $8.4 < M_{\mu^+\mu^-} < 11.1$ GeV/c^2, which in fact includes two observed events. The additional event at 11.5 GeV/c^2 is interpreted as continuum background with 65% probability, or as part of the peak corresponding to known T states with 1% probability. With 90% confidence, there are fewer than 3.5 events above the continuum.

(rms) and 22%, respectively, and the simulated T cross section is normalized to the γGF value described above. The reconstructed peak corresponding to $10^4\times$ the expected signal is shown in Fig. 4; 1.0 events from all T states are expected in the data. Our 3.8-event limit, integrated luminosity, and detection efficiency combine to set the 90%-confidence limit $\sigma(\mu N \to \mu TX)B(T \to \mu^+\mu^-) < 22\times10^{-39}$ cm^2. With $B(T \to \mu^+\mu^-) = (3.1\pm0.9)\%[29]$, we obtain the 90%-confidence cross-section limit $\sigma(\mu N \to \mu TX) < 0.79\times10^{-36}$ cm^2, including the error in the branching ratio. This limit lies above published predictions which use either the vector-meson dominance[30,31] or the γGF[32] models. Ignoring any γGF model uncertainty, this result rules out the choice $|q_b| = 2/3$ with 85% confidence. With 67% confidence, the data disfavor the existence of similar bound states of a second charge 1/3 quark in the T mass region.

F. Original ψ-Muoproduction Results

The analysis in our early ψ publication[3] found the elastic data to be in agreement with a t-dependence of the form

$$d\sigma/dt\,(\gamma Fe \to \psi X) = G(t)d\sigma/dt\,(\gamma N \to \psi N)\,(t=0),$$

$$G(t) = A_e^2\exp(\alpha t) + A_e[(1-\varepsilon\delta)\exp(\beta t) + \varepsilon\delta\exp(\delta t)],$$

with nuclear shadowing factor $A_e = 0.9$, coherent slope $\alpha = 150$ (GeV/c)$^{-2}$, incoherent slopes $\beta(\delta) = 3(1)$(GeV/c)$^{-2}$, and $\varepsilon = 1/8$. Very recent fits now being finalized for publication have determined from the data alone a coherent fraction and average incoherent slope which are in close agreement with the above. All ψ results which I shall mention are corrected to a free-nucleon target.

In the initial publication[3], we observed a Q^2-dependence roughly consistent with ψ dominance ($\Lambda = 2.7\pm0.5$ GeV/c^2). The observed ν-dependence of the effective cross section was in disagreement with the the available γGF prediction[33]. Subsequently, Weiler[34] and Barger, Keung and Phillips[28] obtained much better agreement with the data by parameterizing the gluon distribution as $C(1-x)^n/x$ at gluon four-

momenta-squared of order $m_\psi{}^2$, rather than at smaller values. They fit $n=5.6^{+0.8}_{-1.2}$, and $n=4.6$, respectively; the latter authors found the observed Q^2-dependence to be consistent with $m_c=1.5$ GeV/c^2. At present, we are preparing for publication final combined fits to n and m_c. These fits favor significantly smaller m_c and larger n than mentioned above; I urge caution in use of the results of Refs. 34 and 28.

G. Polarization and Q^2-Dependence of Elastic ψ Muoproduction

Recently, we have measured[4] the polarization of muoproduced $J/\psi(3100)$, analyzed by the decay $\psi \to \mu^+\mu^-$. These are the first data on the polarization of any charmonium state produced by real or virtual photon-nucleon collisions. Measurement of the ψ polarization is an essential component of the study of ψ-leptoproduction mechanisms. If ψ-N elastic scattering is helicity-conserving, the polarization of elastically leptoproduced ψ's in the vector-meson-dominance (VMD) picture[35] is simply related to that of the exchanged photon. In this case, the data measure R, the ratio σ_L/σ_T of ψ production cross sections by longitudinally and transversely polarized virtual photons (γ_L and γ_T). Since R must vanish at $Q^2=0$, it is a function of Q^2 which must be incorporated in any complete description of the Q^2-dependence of ψ leptoproduction.

Some aspects of the apparatus and analysis have been described briefly in sections B and F. For 3μ final states, the trigger demanded ≥ 3 hits in each of 3 consecutive trigger scintillator banks (Fig. 1). The trigger efficiency was uniform near the ψ mass, with a threshold below ~ 1 GeV. A typical mass spectrum of $\mu^+\mu^-$ pairs already has been exhibited in Fig. 4. The analysis discussed in this section used a different muon pairing algorithm, which usually chose the unpaired muon to be the more energetic. Whenever the two like-sign muons differed by more than a factor of 2 in energy, the unpaired muon was chosen to make the smaller laboratory angle with the beam track. This pairing

algorithm retained 92% of the Monte Carlo ψ's in the mass peak, dis-
persing the remainder in a broad spectrum between 0.7 and 6 GeV, with-
out producing important distortions in distributions of other variables.

The angular distributions of the decay products of lower-mass
vector mesons[36] have been shown to be consistent with s-channel heli-
city conservation (SCHC) and natural parity exchange (NPE). With these
assumptions, the distribution of dimuons from ψ decay is[37]

$$W(n,R;\theta,\phi)=[3/16\pi(1+\epsilon R)]\{1+\cos^2\theta+\epsilon(2R-n\cos2\phi)\sin^2\theta+F\sin2\theta\}.$$

Here θ is the polar angle of the like-sign daughter muon in the ψ rest
frame, with $\theta=\pi$ in the direction of target recoil. The azimuthal
"polarization angle" in this "helicity frame" is $\phi=\cos^{-1}(\hat{n}_d\cdot\hat{n}_p)-$
$\cos^{-1}(\hat{n}_p\cdot\hat{n}_s)$, where $\hat{n}_s$, $\hat{n}_p$, and $\hat{n}_d$ are the unit normals to the incident
muon scattering, ψ photoproduction, and ψ decay planes, respectively.
We use ϵ to denote the ratio of γ_L to γ_T fluxes, and introduce the fac-
tor n to monitor the size of the $\cos2\phi$ term: $n=1$ if SCHC and NPE are
exactly obeyed. The function F, arising from the single spin flip ele-
ments of the density matrix, produces effects too small to be observed
in these data.

To avoid statistical problems with low bin populations we have
folded θ and ϕ into one quadrant, eliminating any sensitivity of W to
F. The data were divided into a 4×5×3 grid in Q^2, $|\cos\theta|$, and
$\phi_F=\frac{1}{2}\cos^{-1}|\cos2\phi|$; dimuon-mass-continuum subtractions were performed in
each of the 60 bins to obtain the acceptance-corrected ψ yields dis-
played in Table 1. Using the simulated average true values of Q^2, ϵ,
$\cos^2\theta$, and $\cos2\phi$ for each bin, these yields were fit to the product of
$W(n,R)$ and the propagator $P(\Lambda)\equiv(1+Q^2/\Lambda^2)^{-2}$. Thereby, allowance was
made for the possibility that the decay angular distribution is a
function of Q^2 through the Q^2-dependence of R, e.g. $R\propto Q^2/m_\psi^2$ as sug-
gested[35] by VMD. Since the experimental acceptance is not uniform in
$\cos\theta$, such a dependence could have biased our measurement of Λ if the

TABLE 1. Effective cross section, differential in $\cos\theta$ and ϕ, for the reaction $\gamma_V Fe \rightarrow \psi X$ (energy(X)<4.5 GeV), in arbitrary units. Data and statistical errors are given in 60 bins, defined by average Q^2 (top row), average $\cos^2\theta$ (left column), and one of three ϕ bins (second-left column). The average $\cos 2\phi$ in each ϕ bin is given vs. $<Q^2>$ in the bottom three rows; values of average ε are in the right column. At lowest Q^2, average $\cos 2\phi$ in ϕ bin 1 (2) grows by 0.32 (0.23) as $\cos^2\theta$ rises from 0.02 to 0.54. The variation of average $\cos 2\phi$ with $\cos^2\theta$ is much weaker in other bins, and negligible at highest Q^2.

$<Q^2>$(GeV/c)^2		0.10	0.53	1.60	6.34	
$\overline{\cos^2\theta}$	ϕ bin	$d^2\sigma$(eff)/$d\phi d\cos\theta$(arbitrary units)				$<\varepsilon>$
0.02	1	0.52(07)	0.37(09)	0.30(10)	0.05(07)	
	2	0.55(07)	0.61(11)	0.36(11)	0.10(05)	0.82
	3	0.59(06)	0.64(13)	0.44(09)	0.35(11)	
0.06	1	0.51(06)	0.24(07)	0.36(13)	0.05(04)	
	2	0.61(07)	0.68(13)	0.35(10)	0.27(10)	0.81
	3	0.50(06)	0.76(14)	0.54(11)	0.22(06)	
0.16	1	0.54(07)	0.25(11)	0.22(10)	0.04(05)	
	2	0.64(08)	0.52(12)	0.36(11)	0.09(04)	0.80
	3	0.52(07)	0.56(11)	0.49(11)	0.11(05)	
0.32	1	0.58(08)	0.32(12)	0.36(13)	0.04(06)	
	2	0.46(08)	0.47(16)	0.27(09)	0.12(07)	0.76
	3	0.62(09)	0.66(14)	0.39(10)	0.11(06)	
0.54	1	0.55(28)	0.91(34)	0.31(25)	0.12(10)	
	2	0.67(20)	0.15(28)	0.48(22)	0.05(10)	0.65
	3	1.09(29)	1.21(48)	0.35(28)	0.12(10)	
$\overline{\cos 2\phi}$	1	-0.09	0.54	0.73	0.80	
	2	-0.26	-0.11	-0.07	-0.03	
	3	-0.46	-0.72	-0.74	-0.81	

XBL 809-11762

the data had been summed over all angles.

The details of the fits are presented in Table 2. Three-parameter fits to η, R, and Λ are made both with $R \propto Q^2$ (fits 1 and 6) and with R=constant over the Q^2 range (fit 2). The parameter Λ describes the Q^2-dependence of the effective sum $\sigma_{eff} = \sigma_T + \varepsilon\sigma_L$ of γ_T and γ_L cross sections, or, in the case of fit 6, only of σ_T. An additional complication is the possible Q^2-dependence of any nuclear shadowing in the Fe target. We have used data which recently were summarized[38] for $A \approx 200$, scaled the data to A=56, and fit a universal curve in $x^\prime \equiv Q^2/(2m_M\nu + m_N^2)$:

$$A_{eff}/A(Fe) \equiv S(x^\prime) = (1-0.33\exp(-28x^\prime))^{0.76}.$$

All fits in Table 2 are made both with $S(x^\prime)$ included (multiplying W) and ignored.

The results of fits 1-4 are shown in Fig. 5. For purposes of this display only, the data and fits plotted vs. $|\cos\theta|$ (ϕ_F) are summed over ϕ_F ($|\cos\theta|$). The main feature of these angular distributions is a strong dependence upon ϕ_F, in the form predicted by SCHC. Unpolarized ψ's would yield a flat angular distribution (fit 3), which is ruled out. The data show no strong dependence on $|\cos\theta|$, slightly disfavoring R=0 (fit 4); significant Q^2-dependence of R is not required (fit 2). The photon-gluon-fusion (γGF) model[26], which has successfully described[28,34] other features of elastic ψ muoproduction, has yielded no prediction for the ψ polarization. This is due in part to complications associated with the exchange, required by color conservation, of at least two vector gluons.

Figure 6 presents the Q^2-dependence of σ_{eff}, summed over ν and normalized to unity at Q^2=0. For purposes of this display only, the data and fits to Λ are summed over $|\cos\theta|$ and ϕ_F. When the angular distribution is parameterized in the SCHC form with $R \propto Q^2$ and $S(x^\prime)$ included, $\Lambda = 2.03^{+0.18}_{-0.12}$ GeV/c^2, where the statistical errors take into ac-

TABLE 2. Fits to the Q^2, ϕ, and θ-dependence of the effective cross section σ_{eff} for the reaction $\gamma_V \text{Fe} \rightarrow \psi X$ (energy$(X) < 4.5$ GeV). The angular function $W(\eta, R)$, propagator $P(\Lambda)$, and nuclear screening factor $S(x^-)$ are defined in the text. Each of seven fits (numbered in the first column) is performed both with $S(x^-)$ included (multiplied "in") and ignored ("out") in the function fitted. Values of chi-squared and the degrees of freedom are given in the fourth column. Errors on the fit parameters Λ, η, and ξ^2 (fits 1 and 6) or R (fit 2) are statistical. Fit 6 is the same as fit 1 except that W is multiplied by $(1+\epsilon R)$; Λ then parameterizes the Q^2-dependence of σ_T rather than σ_{eff}. Fit 7 compares the data integrated over ϕ and $\cos\theta$ with the Q^2-dependence predicted by γGF.

Fit No.	Function	$S(x^-)$	χ^2/DF	$\Lambda(\text{GeV/c}^2)$	η	ξ^2 or R
1	$W(\eta,R) \times P(\Lambda)$	in	45.4/56	$2.03^{+0.18}_{-0.12}$	$1.02^{+0.28}_{-0.23}$	$3.3^{+4.9}_{-3.0}$
	$R = (\xi Q/m_\psi)^2$	out	45.5/56	$2.18^{+0.18}_{-0.13}$	$1.04^{+0.28}_{-0.23}$	$4.0^{+4.8}_{-3.4}$
2	$W(\eta,R) \times P(\Lambda)$	in	42.0/56	2.24 ± 0.13	$1.09^{+0.31}_{-0.24}$	$.35^{+.26}_{-.18}$
	$R = $ constant	out	42.4/56	2.43 ± 0.15	$1.10^{+0.31}_{-0.24}$	$.37^{+.27}_{-.22}$
3	$1 \times P(\Lambda)$	in	73.3/58	2.06 ± 0.11		
		out	73.3/58	2.22 ± 0.13		
4	$W(1,0) \times P(\Lambda)$	in	48.6/58	2.21 ± 0.12	$\equiv 1$	$\equiv 0$
		out	49.3/58	2.40 ± 0.14		
5	$W(\eta,0) \times P(m_\psi)$	in	89.1/58	$\equiv 3.1$	0.96 ± 0.13	$\equiv 0$
		out	68.5/58		0.93 ± 0.14	
6	$(1+\epsilon R) \times$Fit 1	in	47.0/56	2.08 ± 0.24	0.86 ± 0.17	$.24^{+.61}_{-.39}$
		out	47.6/56	2.20 ± 0.29	0.87 ± 0.17	$.34^{+.75}_{-.43}$
7	γGF -- Q^2 projection	in	32.1/8	$m_c \equiv 1.5$ GeV/c^2		
		out	14.6/8			
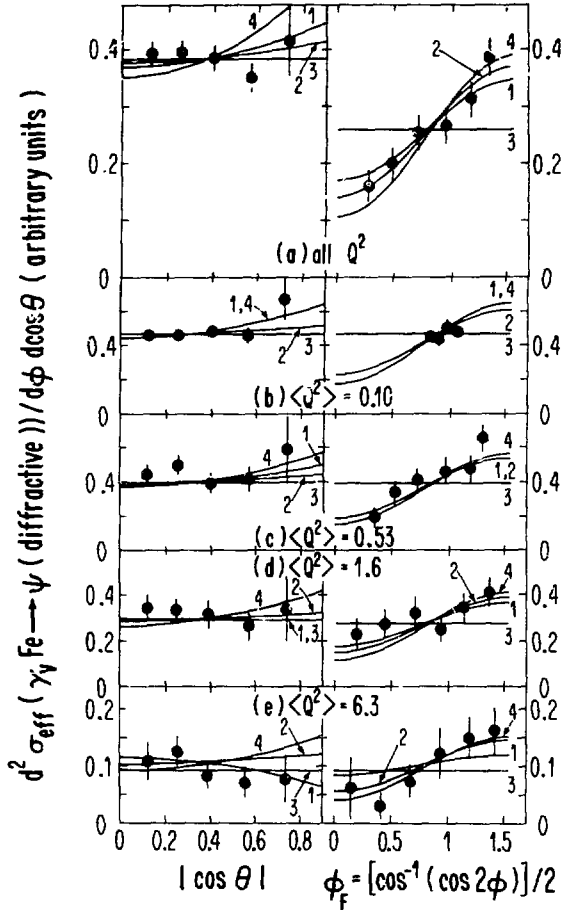
XBL 809-1801

FIG. 5. Angular dependence of the effective cross section for the reaction $\gamma_V \text{Fe} \to \psi X$ (energy(X)<4.5 GeV). Data and statistical errors are presented vs. $|\cos\theta|$ (left column) and ϕ_F (right column), with $\phi_F = \phi$ folded into one quadrant; θ and ϕ are defined in the text. All data ($<Q^2>=0.71$) are shown in (a); (b)-(e) divide the data into four Q^2 regions. Numbered solid lines exhibit the results of fits 1-4 in Table 2. Fits 1, 2, and 4 are to the SCHC formula with $\sigma_L/\sigma_T = \epsilon^2 Q^2/m_\psi^2$, constant, and zero, respectively; fit 3 corresponds to the production of unpolarized ψ's. Each fit is made to all the data with one adjustable normalization constant.

- 19 -
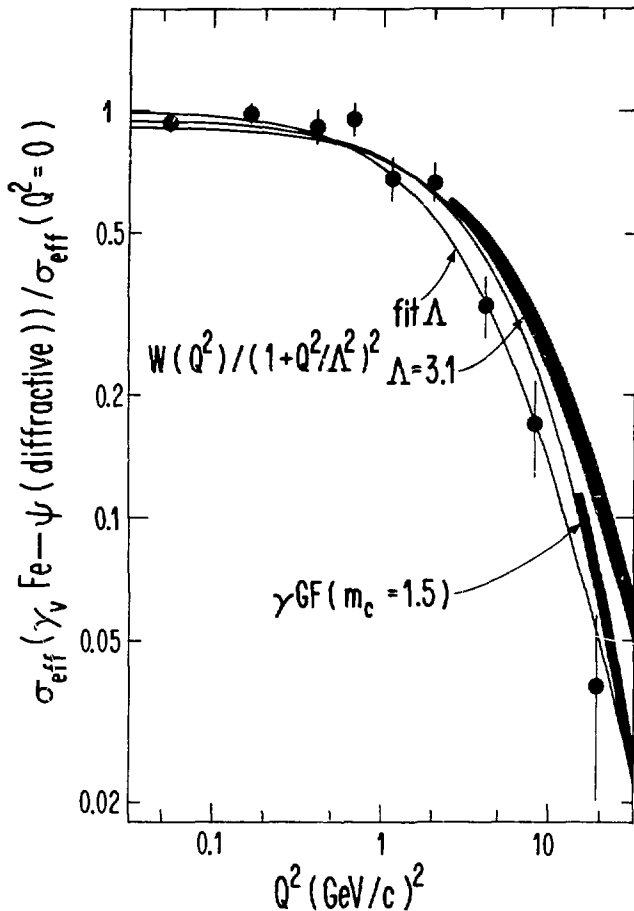
XBL 808-1800

FIG. 6. Q^2-dependence of the effective cross section for the reaction $\gamma_v Fe \rightarrow \psi X$ (energy(X)<4.5 GeV). Statistical errors are shown. Typical Q^2 resolution is 3.1 (0.6) $(GeV/c)^2$ at $Q^2=17$ (1.2) $(GeV/c)^2$. The data are fit to $(1+Q^2/\Lambda^2)^{-2}$ multiplied by the function $W(\eta, R)$ shown in Table 2. The weak Q^2-dependence of W results from the Q^2-dependence of $R=\sigma_L/\sigma_T$ and the particular average values of the angular factors $\cos^2\theta$ and $\cos 2\phi$, as given in Table 1. The best fits with free Λ (Table 2, fit 1) and fixed $\Lambda=3.1$ (Table 2, fit 5) are shown. The data are normalized so that fit 1 is unity at $Q^2=0$. Also exhibited is the γGF prediction (Table 2, fit 7). At high Q^2, the two latter fits are displayed as a solid band, with the upper (lower) edge including (omitting) the screening factor $S(x^-)$.

- 20 -

count the uncertainties in η and ξ^2 (Table 2, fit 1). If instead R=constant and $S(x')$ is left out, Λ=2.43±0.15 GeV/c^2 (fit 2). The other fits to Λ, either for σ_{eff} or σ_T (fit 6), are within this ±0.2 GeV/c^2 range, which accounts for the principal systematic error in Λ. We conclude that Λ is between 1.9 and 2.6 GeV/c^2. The simplest VMD prediction, Λ=m$_\psi$ (fit 5), is ruled out.

We also have fit the data in Fig. 6 to the γGF prediction (fit 7), assuming a charmed quark mass m$_c$=1.5 GeV/c^2 and a gluon distribution $G(x)=3(1-x)^5/x$. The data fall faster than the γGF curve, giving a barely acceptable fit (7% confidence) only if $S(x')$ is omitted. We have reached a similar conclusion[6] comparing γGF predictions with open charm muoproduction, using a different analysis. Varying m$_c$ and the exponent of $(1-x)$ in $G(x)$ improves the γGF fit. We are in the process of making a combined determination of these parameters using the Q^2 and ν spectra of the ψ data.

To summarize this section, the azimuthal-angle distributions for muoproduced $\psi\rightarrow\mu^+\mu^-$ decay demonstrate that the reaction $\gamma_V N\rightarrow\psi N$ is helicity-conserving, and the polar-angle distributions suggest some longitudinally-polarized production, but do not rule out R=0. The Q^2-dependence of either σ_{eff} or σ_T clearly is steeper than $(1+Q^2/m_\psi^2)^{-2}$.

H. Cross Sections for Charm Production by Muons and Photons

The measurement of charm production in this experiment is similar to that in most neutrino experiments[39]. Charm states are identified by their $\geq$3-body decay into muons. Specified charmed hadrons are not resolved; they appear in the data weighted by their production cross section and leptonic branching ratio. This "continuum" signal is not well adapted to first observation[40] of charmed states, nor to the study of their decay systematics. However, once discovered in other reactions, charm production offers the only reasonable explanation for all but (19±10)% of the 20072 fully reconstructed single-extra- muon final states

reported here. These statistics and signal-to-background level together with unambiguous determination of virtual-photon four-momenta make possible the study of charm-production mechanisms.

The $\geq 2\mu$ trigger required a $\gtrsim 20$-GeV hadronic shower $\gtrsim 2m$ upstream of ≥ 2 hits in each of three successive trigger hodoscopes (Fig. 1). Full tracking capability in an area including the beam produced a high, nearly Q^2-independent acceptance. In the analysis of same-sign dimuons, the more energetic muon was chosen to be the scattered muon. As inferred from $\mu^+\mu^-$ final states where the choice is obvious, this algorithm is successful for 91% of the same-sign events. The calorimeter was calibrated using the momentum-analyzed energy loss of high Q^2 single-muon triggers with a ≈ 3 GeV correction for the presence of a second muon.

Several analysis cuts were made to exclude regions of rapidly varying acceptance. Daughter muon energies were required to exceed 15 GeV, reconstructed vertices to fall between the centers of the first and eighth modules (Fig. 1), and hadronic shower energies to exceed 36 GeV. To avoid contamination from low-mass electromagnetically-produced muon pairs, the daughter muon was required to possess at least 0.45 GeV/c of momentum transverse to the scattered muon direction.

Monte Carlo charm events were simulated using the γGF model described in section D. For incoherent events the dependence on $-t$, not predicted by the model, was assumed to be as measured in the same apparatus for ψ production[3]. Likewise, the same nuclear parameters were used for coherent events. Carrying the full photon energy, charmed quark pairs with invariant mass exceeding the mass of two D mesons were transformed to D mesons using a fragmentation function $D(z) = (1-z)^{0.4}$ consistent with SPEAR data[41]. Here, z is the fraction of the parent quark's energy received by the charmed meson in the $c\bar{c}$ center of mass. The simulation assumed that neutral and charged D's are produced in a

2:1 ratio and decay to muons[42] with 4% and 20% branching ratios, respectively[43]. Production and decay of other charmed states were not explicitly simulated. These numbers imply a yield of 0.187 decay muons per charmed-quark pair. The $K\mu\nu$ ($K^*\mu\nu$) branching ratios were taken[43] as 0.61 (0.39). Charm decays to electrons with the same branching ratios were included to model missing energy from electron as well as muon neutrinos.

The major background to charm production is decay in flight of muoproduced π and K mesons. The corresponding Monte Carlo simulation used inelastic structure functions parameterized by the Chicago-Harvard-Illinois-Oxford collaboration[44]. From the same experiment[45] π and K production data were used to determine final state particle multiplicities and momentum distributions. Bubble chamber data[46] were used to parameterize secondary interactions between mesons in the showers and nucleons in the target. Because of this experimental input the Monte Carlo was free from dependence on models of hadron production. Showers were allowed to develop until no hadron energy exceeded 5 GeV. Hadron trajectories were simulated in the same detail as muon trajectories. The small yield of prompt muons from ρ decay, Drell-Yan processes and hadronic charm production in showers was neglected. The decay simulation was compared with a Caltech-Fermilab-Rockefeller (CFR) neutrino experiment's shower Monte Carlo[47], based in part on a model of hadron production. The CFR Monte Carlo predicted a rate 15% (35%) higher at W-boson energy of 130 GeV (180 GeV) than did this experiment's calculation for similar virtual photon energies.

To improve the ratio of signal to background, data with $\nu<75$ GeV were excluded. With this cut, absolute normalization of the π,K-decay Monte Carlo to the integrated beam flux fixes this background at 19% of the sample. The systematic normalization uncertainty in the shower Monte Carlo is determined to be $\pm50\%$ in part by comparing the calculated

π, K fraction with that obtained by representing the data as a combination of simulated π, K decay and charm events.

After the π,K-decay background is subtracted bin-by-bin from the data, the charm signal and the γGF prediction are compared in Fig. 7 (a)-(f). The muon-scattering vertex is modeled precisely in ν and adequately in Q^2. The longitudinal decay-muon variables (c) and (d) are in satisfactory agreement, as is the missing energy within the calorimeter calibration uncertainty. The daughter muon $p_\perp$ is higher in the data by 15%; however, this variable is sensitive to details of -t slope and charm decay systematics, which are not model predictions. Overall, the γGF model is an adequate basis for acceptance calculation.

Barger, Keung and Phillips[48] have discussed the potential background due to feed-down of trimuon final states due to electromagnetic production of muon pairs in which one muon is undetected. With our calorimeter energy requirement, their calculation predicts less than a 5% contamination from this source. Independently, contamination from feed-down of any background source of trimuons was checked by blinding the analysis to the softest muon in all detected trimuon final states otherwise satisfying the dimuon trigger and analysis requirements. These events, comprising 3.9% of the normal sample, amount to 100.1±5.3% of the Monte Carlo yield of detected muon decays from both D mesons. Thus, any other processes generating trimuons with the same muon detection efficiency as the charm signal can account for no more than 0.5% of the data. A standard calculation of $\tau\bar{\tau}$ production[48] and our γGF calculation of bottom quark pair production limit these "contaminants" to less than 0.1% and 0.03% of the sample, respectively.

The spectrometer's acceptance is by far most sensitive to the energy spectrum of produced muons. The γGF model describes quasielastic $c\bar{c}$ production[26] and predicts a ν distribution in excellent agreement with that observed in the subtracted data. Therefore, most of the model
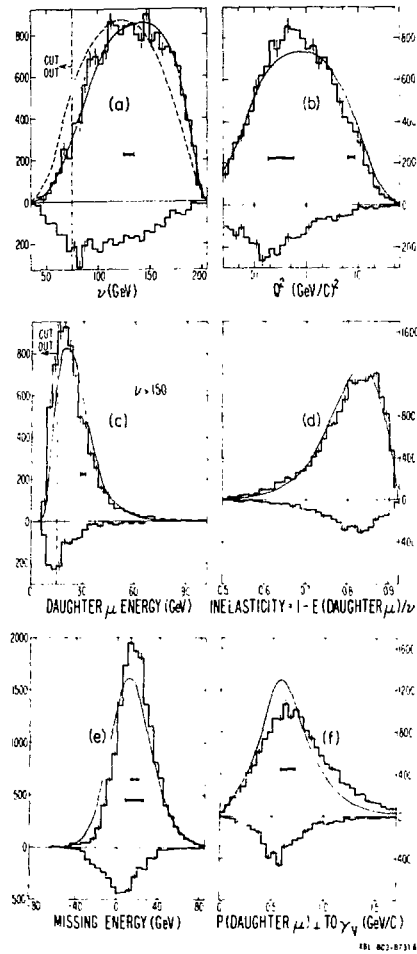
FIG. 7. Reconstructed distributions in (a) energy transfer, (b)
momentum-transfer-squared, (c) daughter muon energy. (d) inelasticity,
(e) missing (neutrino) energy, (f) daughter muon $p_\perp$. The ordinates are
events per bin with acceptance not unfolded. Inverted histograms show
the simulated π, K-decay background, absolutely normalized to the in-
tegrated beam flux. Erect histograms exhibit data after subtraction
of this background; statistical errors are shown. The curves, normal-
ized to the subtracted data, are the photon-gluon-fusion charm calcu-
lation. The dashed curve in (a) represents an alternate model in which
$D\bar{D}$ pairs carrying the full photon energy are produced with a probabil-
ity independent of ν. Events in (c) have $\nu > 150$ GeV. The horizontal
brackets exhibit typical apparatus resolution (rms). The arrow in
(e) shows the shift caused by a $\pm 2.5\%$ excursion in calorimeter cali-
bration.

dependence introduced in the analysis may be studied by varying the
daughter muon energy distribution through changes in $D(z)$. Remodeling
detector acceptance with $D(z)=(1-z)^3$ $(D(z)=(1-\min(z,0.99)^{-1.5})$ predicts
mean daughter energies in five-standard-deviation disagreement with sub-
tracted data and decreases (increases) the calculated acceptance by a
factor of 1.24 (1.20). The agreement between subtracted data and γGF
Monte Carlo is substantially worsened in many other distributions. The
systematic errors quoted below are the sum in quadrature of excursions
caused by the π, K normalization uncertainty and the fragmentation-
induced changes in acceptance. After a relative acceptance correction
of 26%, the ratio of opposite- to same-sign daughter muon events is
1.066±0.028 (±0.055), where the latter error is systematic.

The measured cross section for diffractive charm production is

$$\sigma_{\text{diff}}(\mu N \rightarrow \mu c \bar{c} X) = 6.9^{+1.9}_{-1.4} \text{ nb.}$$

"Diffractive production" refers to creation of $c\bar{c}$ pairs carrying most
of the laboratory energy of the virtual photon, as in the γGF, VMD, and
otehr peripheral models. The present analysis is insensitive to other
possible mechanisms produced charm nearly at rest in the virtual photon-
nucleon center of mass. This cross section is 137% of the γGF pre-
diction. Corrected by a factor of 1.45 for the different beam energy,
it is three times the cross section reported by the Michigan State-
Fermilab group[49].

The muon cross section is expressed as an effective photon cross
section σ_{eff} by factoring out the equivalent flux[50] of transversely
polarized virtual photons. Figures 8 (a) and (b) show the extrapolation
of σ_{eff} to $Q^2=0$ using a VMD propagator. The best-fit χ^2 values are
approximately 1.8 per degree of freedom, due in part to a tendency for
σ_{eff} to rise slightly with Q^2 near $Q^2=0.2$ (GeV/c)^2. Allowing for sys-
tematic error, the best fit propagator masses are $\Lambda=3.3\pm0.2$ and
2.9 ± 0.2 GeV/c^2 at $\nu=178$ and 100 GeV, and the intercepts at $Q^2=0$ are
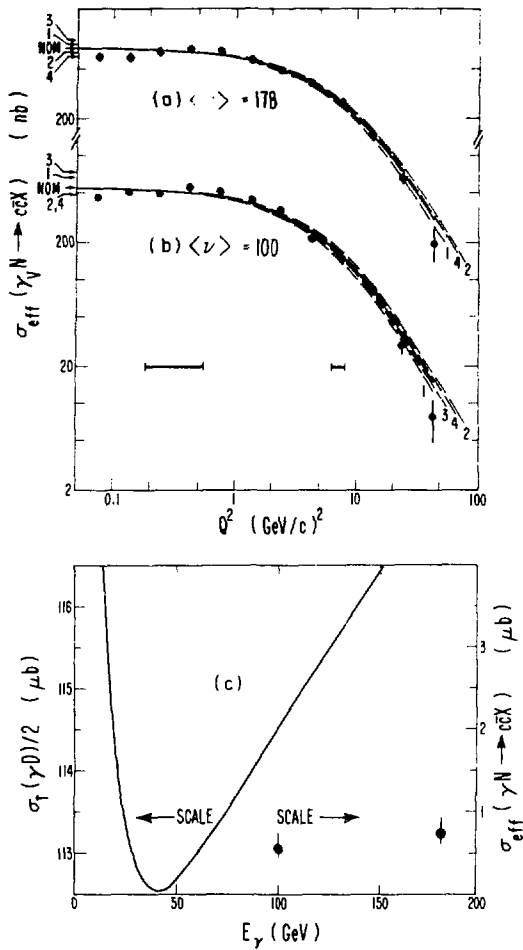
FIG. 8. Diffractive charm photoproduction cross sections and the rise of the photon-nucleon total cross-section. Parts (a) and (b) exhibit the extrapolation of the effective cross section for diffractive charm photoproduction to $Q^2=0$ at $\nu=$ (a) 178 and (b) 100 GeV. Statistical errors are shown. The solid curves are fit to $\sigma_0(1+Q^2/\Lambda^2)^{-2}$ with $\Lambda=$ (a) 3.3 and (b) 2.9 GeV/c; the arrows labelled "NOM" exhibit σ_0. Systematic errors are parameterized by (1) decreasing, (2) increasing by 50% the subtracted π, K-decay background, and by recalculating the acceptance with a (3) softer, (4) harder quark fragmentation function as described in the text. Systematic effects on σ_0 are indicated by numbered arrows and effects on Λ are indicated by dashed curves, normalized to the same σ_0. Part (c) compares the extrapolated cross-sections for diffractive charm production by real photons (data points, right scale) with a fit (Ref. 51) to $\frac{1}{2}\sigma_T(\gamma d)$ (curve, left scale).

750^{+180}_{-130} and 560^{+200}_{-120} nb, respectively. The rise with ν of 190^{+34}_{-52} nb in the charm photoproduction cross section is significant, while the difference of 0.39 ± 0.18 GeV in propagator masses is only suggestive. In all cases but the last, allowances for systematic uncertainties dominate the errors. The diffractive charm production rate is too small to saturate the rise[51] of the total γN cross section above 50 GeV (Fig. 8 (c)).

We have published[3] a value of 60 ± 20 nb/GeV^2 for $d\sigma/dt$ ($\gamma N \rightarrow \psi N$) at $t=0$ and $\nu=100$ GeV. With the observed -t slope, this corresponds to an elastic cross section of 25 ± 8 nb. The results reported here fix the ratio of elastic ψ to diffractive charm production at $0.045\pm.022$. The central value is approximately 2.5 times Sivers, Townsend, and West's VMD prediction[22]; in that particular picture our result would suggest that non-diffractive charm production may account for a significant fraction of the total charm-photoproduction cross section. Independent of VMD, using the results of Ref. 22, we obtain the 90%-confidence lower limit $\sigma_{total}(\psi N) \geq 0.9$ mb.

For the purpose of discriminating between charm-production models, Fig. 9 displays in more detail the dependence of σ_{eff} on ν in a range of Q^2 centered at 0.75 (GeV/c)^2. The insensitivity of σ_{eff} to Q^2 in this range decouples its Q^2- and ν-dependence. Again, the γGF model with gluon distribution $3(1-x)^5/x$ successfully describes the observed ν-dependence. However, as illustrated by the shaded band, systematic uncertainties prevent the data from ruling out the BN model[25], or the two alternate choices indicated for the gluon x distribution. The precision is sufficient to disfavor a flat ν-dependence.

I. The Charm Structure Function and Its Role in Scale-Noninvariance

The original signature[52] for scale-noninvariance in muon-nucleon scattering was the "shrinkage" of the structure function $F_2(x_B)$ with rising Q^2. As confirmed by subsequent muon[44] and neutrino[53] experiments, $\partial F_2/\partial Q^2$ is positive for fixed Bjorken $x_B \leq 0.1$ and negative for $x_B \geq 0.25$.
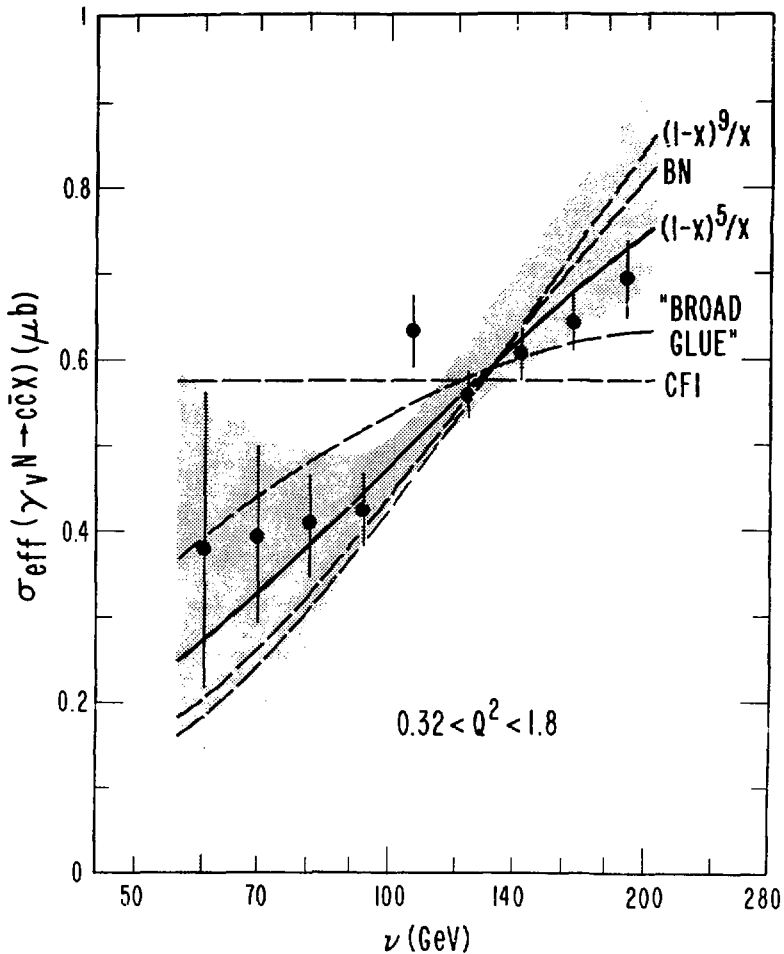
- 29 -

FIG. 9. Energy-dependence of the effective cross section σ_{eff} for diffractive charm photoproduction. For $0.32 < Q^2 < 1.8$ $(GeV/c)^2$, σ_{eff} varies with Q^2 by $\leq 20\%$. Errors are statistical. The solid curve exhibits the ν-dependence of the photon-gluon-fusion model with the "counting-rule" gluon x distribution $3(1-x)^5/x$, and represents the data with 13% confidence. Other gluon-distribution choices $(1-x)^9/x$, and "broad glue" $(1-x)^5(13.5+1.07/x)$ are indicated by dashed curves. The dashed curve labelled BN is the phenomenological parameterization of Ref. 25, and the dashed line labelled CFI represents the energy-independence assumed by recent photoproduction analyses.

Curves are normalized to the data. The shaded band exhibits the range of changes in shape allowed by systematic error. For clarity it is drawn relative to the solid curve. Data below $\nu = 75$ GeV are cut out.

- 29 -

If higher Q^2 is associated with greater resolving power of the exchanged boson probe, this shrinkage may be visualized as an increase in the number of resolved constituents sharing the nucleon momentum. Despite the general nature of this picture, the lepton-nucleon data have been widely interpreted as early confirmation of the specific predictions of quantum chromodynamics (QCD).

Ambiguities in the interpretation of scale-noninvariance in F_2 are different at high and low x_B. Effects of finite target mass conventionally are absorbed into redefinition[54] of x_B, which critically affects F_2 only at high x_B. "High twist" corrections for phenomena which are coherent over two or more constituents have been parameterized[55] as a power series in $(1-x_B)^{-1}$. These problems motivate the suggestion[56] that the stronger of the QCD predictions for F_2 is to be found at low x_B. However, available lepton beam energies limit Q^2 for $x_B \lesssim 0.1$ to values not greatly exceeding $m_{c\bar{c}}^2$. The proximity of this charm mass scale threatens to disrupt any low-x_B study of asymptotic scale-noninvariance. Earlier experimentation has provided only one estimate[57] of the charm contribution to F_2. It was given as a function of two phenomenological parameters which were not quantitatively determined.

In order to discuss the Q^2-dependence of charm muoproduction in connection with inclusive muon scattering, we define the charm structure function $F_2(c\bar{c})$ through the relation

$$Q^4 \nu d^2\sigma(c\bar{c})/dQ^2 d\nu = 4\pi\alpha^2(1-y+y^2/2)F_2(c\bar{c}).$$

Here y is ν/ν_{max} and $\sigma(c\bar{c})$ is the cross section for diffractive charm-pair production in muon-nucleon collisions. We label $\sigma(c\bar{c})$, $F_2(c\bar{c})$, and σ_{eff} as "diffractive" quantities because the analysis is sensitive mainly to $c\bar{c}$ pairs which carry off most of ν. In charm production $F_2(c\bar{c})$ plays the same role as would F_2 in inclusive scattering, if absorption of longitudinally polarized photons were negligible.

Figure 10 exhibits the dependence of $F_2(c\bar{c})$ on Q^2 at two values of
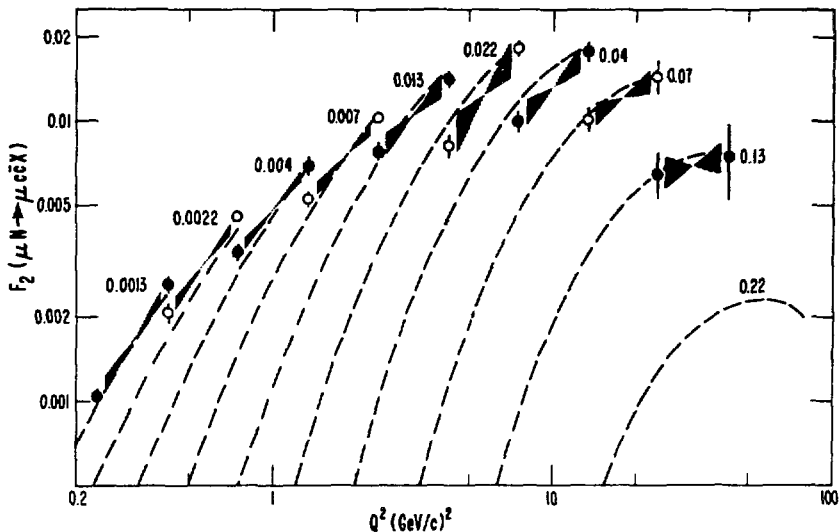
XBL 803-382
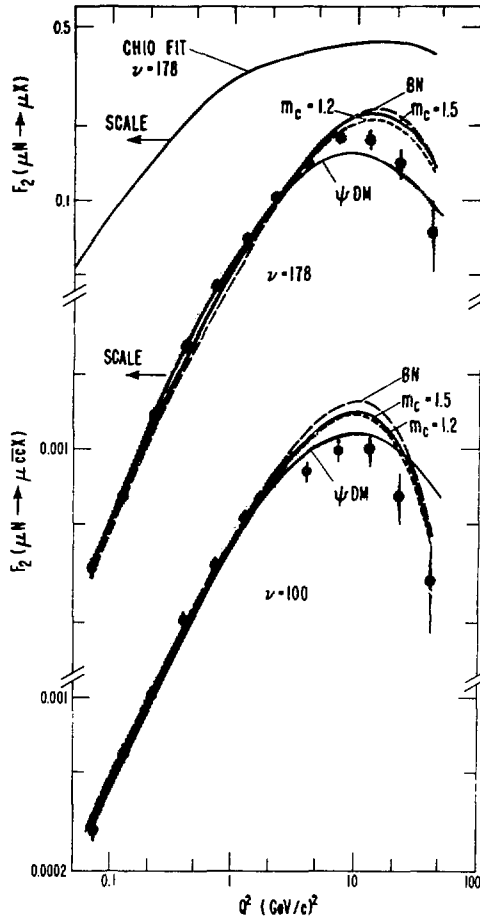
FIG. 10. Q^2-dependence of the structure function $F_2(c\bar{c})$ for diffract-
ive charm muoproduction. At each of the two average photon energies,
each curve is normalized to the data. Errors are statistical. The
solid (short dashed) curves labelled m_c=1.5 (1.2) exhibit the photon-
gluon-fusion prediction with a charmed quark mass of 1.5 (1.2) GeV/c^2.
Solid curves labelled ψDM correspond to a ψ-dominance propagator, and
long-dashed curves labelled BN are the model of Ref. 25. Shown at the
top is a fit adapted from Ref. 44 to the inclusive structure function
F_2 for isospin-0 μN scattering. The shape variations allowed by
systematic errors are represented by the shaded bands.

fixed average ν. The charm structure function rises with Q^2 to a maxi-
mum at $Q^2 \approx 10$ $(GeV/c)^2$, above which it falls steeply. At the peak,
$F_2(c\bar{c})$ is $\approx 4\%$ of the inclusive F_2. None of the models depicted in Fig.
10 is an adequate representation of the data. The γGF shapes for
$m_c = 1.5$ and 1.2 GeV/c^2 are nearly degenerate. In that model[26] the Q^2-
dependence is sensitive to $m_{c\bar{c}}$, which in either case is bounded below
by $2m_D$. The maxima predicted by both the γGF and BN models shift with
ν and curve with Q^2 like the data, but occur at values of Q^2 which are
too high. The ψ-dominance predictions drop too slowly at high Q^2.
Systematic errors are only weakly correlated with Q^2 and do not obscure
the disagreement.

In the energy range of the data in Fig. 11, $F_2(c\bar{c})$ is manifestly
scale-noninvariant for $Q^2 \approx 10$ $(GeV/c)^2$, or $x_B \lesssim 0.07$. To model the charm
contribution to F_2 for smaller photon energies, we multiply the γGF-
model normalization by a factor of 1.37 and damp it at high Q^2 by the
arbitrary factor $(1+Q^2/(10\ GeV/c)^2)^{-2}$. The resulting family of dashed
curves in Fig. 11 adequately matches the data where overlap exists.

To describe the full effect of charm production on F_2 we must in-
clude the charmonium contribution. The ψ-muoproduction rate[3] agrees
with the unmodified γGF prediction if elastic ψ production accounts for
$1/6$ of all charmonium production[28]. This is close to the fraction ex-
pected if all charmonia are produced with equal likelihood. Adopting
this model, we augment the measured $6.9^{+1.9}_{-1.4}$ nb open-charm cross section
by 2.8 nb of bound charm production. Since charmonium production falls
more rapidly at high Q^2 than open charm production, this augmentation
increases the charm contribution to inclusive scale-noninvariance only
by $\leq 15\%$ in the region where it is most important.

To focus on the absolute charm contribution, published[44] fits at
fixed x_B to the inclusive $\partial F_2/\partial \ell n Q^2$ are compared in Table 3 to
$\partial F_2(c\bar{c})/\partial \ell n Q^2$ augmented for charmonium production. Although the latter

FIG. 11. Scale-noninvariance of $F_2(c\bar{c})$. Data points are arranged in pairs, alternately closed and open. The points in each pair are connected by a solid band and labelled by their common average value of $x_B = Q^2/2m_p\nu$. Errors are statistical. The dashed lines are the prediction of the photon-gluon-fusion model with $m_c = 1.5$ GeV/c^2 except that the model is renormalized and damped at high Q^2 as described in the text. The solid bands represent the slope variations allowed by systematic errors.

TABLE 3. Calculated $10^4 \partial F_2 / \partial \ell n Q^2$ at fixed x_B vs. ν (top), Q^2 (left margin), and x_B (diagonals, right margin). For each Q^2-ν combination, two values are shown. The bottom value is fit to the structure function F_2 for νN scattering (Ref. 44). The top value is the contribution $F_2(c\bar{c})$ to F_2 from diffractive muoproduction of bound and unbound charmed quarks.

ν(GeV)	27	42	67	105	168	
Q^2 (GeV/c)^2	$\dfrac{10^4 \partial F_2(c\bar{c})/\partial \ell n Q^2}{10^4 \partial F_2(\mu N)/\partial \ell n Q^2}$					x_B
0.63	17 / 1070	30 / 1090	43 / 1110	54 / 1120	58 / 1130	
1.0	23 / 980	43 / 1010	63 / 1040	77 / 1050	84 / 1060	0.002
1.6	30 / 650	59 / 680	87 / 700	107 / 720	116 / 730	0.003
2.5	36 / 310	73 / 340	110 / 350	139 / 360	146 / 360	0.005
4.0	36 / 320	80 / 390	128 / 430	162 / 460	163 / 480	0.008
6.3	29 / 210	75 / 330	128 / 410	.165 / 460	154 / 490	0.013
10	15 / 50	54 / 220	104 / 340	138 / 430	112 / 480	0.020
16	4 / -130	27 / 50	64 / 230	90 / 360	52 / 440	0.032
25	-2 / -189	7 / -126	26 / 50	40 / 230	0 / 370	0.050
40	0 / -31	-1 / -171	6 / -122	10 / 50	-22 / 240	0.080
63	/	0 / -23	1 / -154	1 / -119	-16 / 50	0.130

numbers are calculated rather than measured, we emphasize that the
(γGF) model used has been made to agree with the diffractive charm-
muoproduction data. In the region where charm scale-noninvariance is
most important, the calculation is reliable to $\approx \pm 40\%$.

We conclude from Table 3 that diffractive charm production makes
a contribution to inclusive scale-noninvariance which is very large
compared to the $\lesssim 4\%$ relative magnitude of its cross section. On average,
in a region bounded by $2 < Q^2 < 13$ $(GeV/c)^2$ and $50 < \nu < 200$ GeV and centered
at $\dot{x}_B \approx 0.025$, it contributes 1/3 of the total inclusive scale-noninvari-
ance. This region embraces the data providing most of the original evi-
dence[52] for scale-noninvariance in muon scattering. VMD arguments men-
tioned in section H raise the possibility that substantial non-diffract-
ive charm muoproduction exists in addition to the diffractive production
to which the analysis presented here is sensitive. A portion of any
non-diffractive charm production might add further to the diffractive
scale-noninvariance we have discussed.

We emphasize that the scale-noninvariance created by diffractive
charm muoproduction is not a direct manifestation of asymptotic freedom
or other fundamental theory. It is only a kinematic effect tied to the
scale of the charmed quark mass. To study deeper implications of
scale-noninvariance in muon scattering, one must include this effect in
the model being fit, or subtract it from the data.

J. Acknowledgements

[a]Present address: The Enrico Fermi Institute, 5650 S. Ellis Avenue, Chicago, Illinois 60637.

[b]Present address: Bell Telephone Laboratories, Murray Hill, New Jersey 07974.

[1]A.R. Clark et al., LBL-11663 (1980), submitted to Phys. Rev. Letters.

[2]A.R. Clark et al., Phys. Rev. Lett. 45, 686 (1980).

[3]A.R. Clark et al., Phys. Rev. Lett. 43, 187 (1979).

[4]A.R. Clark et al., LBL-11562 (1980), submitted to Phys. Rev. Letters.

[5]A.R. Clark et al., Phys. Rev. Lett. 45, 682 (1980).

[6]A.R. Clark et al., Phys. Rev. Lett. 45, 1465 (1980).

[7]A.R. Clark et al., in Proceedings of the 1979 International Symposium on Lepton and Photon Interactions at High Energy, edited by T.B.W. Kirk and H.D.I. Abarbanel (Fermilab, Batavia, Illinois, 1979), p. 135-148 (1979).

[8]G.D. Gollin, M.V. Isaila, F.C. Shoemaker, and P. Surko, IEEE Trans. Nucl. Sci. NS-26, 59 (1979).

[9]S. Weinberg, Phys. Rev. Lett. 19, 1264 (1967).

[10]F. Wilczek and A. Zee, Nucl. Phys. B106, 461 (1976).

[11]T. Cheng and L. Li, Phys. Rev. D16, 1425 (1977).

[12]S. Weinberg, Phys. Rev. D5, 1264 (1972); J. Schecter and Y. Ueda, Phys. Rev. D8, 484 (1973); Y. Achiman and B. Stech, Phys. Lett. 77B, 384 (1978).

[13]K.W. Rothe and A.M. Wolsky, Nucl. Phys. B10, 241 (1969).

[14]A.E. Asratyan et al., Phys. Lett. 49B, 488 (1974).

[15]T. Eichten et al., Phys. Lett. 46B, 281 (1973).

[16]B.C. Barish et al., Phys. Rev. Lett. 32, 1387 (1974).

[17]D.J. Bechis et al., Phys. Rev. Lett. 40, 602 (1978). This limit applies only to heavy muons which are long-lived because of some as-yet-undiscovered selection rule.

[18]D.S. Baranov et al., Phys. Lett. 81B, 261 (1979), and Sov. J. Nucl. Phys. 29, 622 (1979).

[19]M.R. Krishnaswamy et al., Phys. Lett. 57B, 105 (1975).

[20]B.C. Barish et al., Phys. Rev. Lett. 38, 577 (1977); A. Benvenuti et al., Phys. Rev. Lett. 38, 1110 (1977).

[21]Q^2 is defined for M^0 production by taking the like-sign final-state muon to be a scattered beam muon.

[22]D. Sivers, J. Townsend, and G. West, Phys. Rev. D13, 1234 (1976).

[23]S. Okubo, Phys. Lett. 5, 160 (1963); G. Zweig, report, 1964 (unpublished); J. Iizuka, Progr. Theor. Phys. Suppl. 37-38, 21 (1966).

[24]D. Bauer et al., Phys. Rev. Lett. 43, 1551 (1979), and references cited therein.

[25]F. Bletzacker and H.T. Nieh, SUNY-Stony Brook Report No. ITP-SB-77-44 (unpublished).

[26]J.P. Leveille and T. Weiler, Nucl. Phys. B147, 147 (1979), and references cited therein.

[27]S. Brodsky and G. Farrar, Phys. Rev. Lett. 31, 1153 (1973).

[28]V. Barger, W.Y. Keung, and R.J.N. Phillips, Phys. Lett. 91B, 253 (1980).

[29]K. Berkelman, summary of DORIS results presented to the XV Rencontre de Moriond (Les Arcs, Savoie, France, March 9-21, 1980).

[30]G. Aubrecht and W. Wada, Phys. Rev. Lett. 39, 978 (1977), make photoproduction predictions which, with γGF ν- and Q^2-dependence assumptions, correspond to 0.15×10^{-36} cm^2 of T muoproduction at 209 GeV.

[31]N. Bralić, Nucl. Phys. B139, 433 (1978), makes leptoproduction predictions which, with γGF energy-dependence assumptions, correspond to 0.07×10^{-36} cm^2 of T muoproduction at 209 GeV.

[32]H. Fritzsch and K. Streng, Phys. Lett. 72B, 385 (1978), make photoproduction predictions which, with γGF ν- and Q^2-dependence assumptions, correspond to 0.36×10^{-36} cm^2 of T muoproduction at 209 GeV.

[33]M. Glück and E. Reya, Phys. Lett. 79B, 453 (1978).

[34]T. Weiler, Phys. Rev. Lett. 44, 304 (1980).

[35]J.J. Sakurai and D. Schildknecht, Phys. Lett. 40B, 121 (1972).

[36]J.T. Dakin et al., Phys. Rev. Lett. 30, 142 (1972); W.R. Francis et al., Phys. Rev. Lett. 38, 633 (1977); R. Dixon et al., Phys. Rev. Lett. 39, 516 (1977).

[37]K. Schilling, P. Seyboth, and G. Wolf, Nuc. Phys. B15, 397 (1970); B. Humpert and A.C.D. Wright, Ann. Phys. 110, 1 (1978); T. Markiewicz, Ph.D. Thesis, Univ. of Calif., Berkeley, 1980 (unpublished).

[38]H. Miettinen, presented at the XX International Conference on High Energy Physics, Madison, Wisconin, July 17-23, 1980.

[39]See, for example, M. Murtagh, in Proceedings of the International Symposium on Lepton and Photon Interactions at High Energies, Batavia, 1979, edited by T.B.W. Kirk and H.D.I. Abarbanel (Fermilab, Batavia, 1979).

[40]G. Goldhaber et al., Phys. Rev. Lett. 37, 255 (1976).

[41]P.A. Rapidis et al., Phys. Lett. 84B, 507 (1979).

[42]We use the decay matrix elements of I. Hinchliffe and C.H. Llewellyn Smith, Nucl. Phys. B114, 45 (1976).

[43]J. Kirkby, in Proceedings of the International Symposium on Lepton and Photon Interactions at High Energies, Batavia, 1979, edited by T.B.W. Kirk and H.D.I. Abarbanel (Fermilab, Batavia, 1979).

[44]B.A. Gordon et al., Phys. Rev. D20, 2645 (1979).

[45]W.A. Loomis et al., Phys. Rev. D19, 2543 (1979).

[46]J.A. Gaidos et al., Nucl. Phys. B23, 10 (1973); P. Bosetti et al., Nucl. Phys. B54, 141 (1973); P. Bosetti et al., Nucl. Phys. B60, 307 (1973); G.A. Akopdjanov et al., Nucl. Phys. B75, 401 (1974); W. Morris et al., Phys. Lett. 56B, 395 (1975).

[47]M. Shaevitz, private communication. The CFR group also studied showers induced by pions incident on their detector.

[48]V. Barger, W.Y. Keung and R.J.N. Phillips, Phys. Rev. D20, 630 (1979).

[49]D. Bauer et al., Phys. Rev. Lett. 43, 1551 (1979).

[50]F.J. Gilman, Phys. Rev. 167, 1365 (1968).

[51]D.O. Caldwell et al., Phys. Rev. Lett. 42, 553 (1979).

[52]Y. Watanabe et al., Phys. Rev. Lett. 35, 898 (1975); C. Chang et al., Phys. Rev. Lett. 35, 901 (1975).

[53]See e.g. J.G.H. deGroot et al., Z. Physik C1, 143 (1979).

[54]See e.g. O. Nachtmann, Nucl. Phys. B63, 237 (1973).

[55]L.F. Abbott, W.B. Atwood, and R.M. Barnett, Phys. Rev. (to be published), and SLAC-PUB-2400 (1979).

[56]F. Eisele, presented at the XV Rencontre de Moriond (Les Arcs, Savoie, France, March 9-21, 1980).

[57]K.W. Chen and A. Van Ginneken, Phys. Rev. Lett. 40, 1417 (1978).